Journal of Materials Chemistry C

ROYAL SOCIETY OF CHEMISTRY

PAPER

View Article Online
View Journal | View Issue

Cite this: J. Mater. Chem. C, 2022, 10, 13964

PEDOT:PSS hydrogel gate electrodes for OTFT sensors†

Joshua N. Arthur, [ab] Samantha Burns,[ab] Cameron M. Cole, [ab] Quinlan T. Barthelme[abc] and Soniya D. Yambem *[abc]

Received 18th March 2022,
Accepted 21st June 2022

DOI: 10.1039/d2tc01096h

rsc.li/materials-c

Organic thin film transistors (OTFTs) have been extensively investigated for biosensing and bioelectronic applications. The conducting polymer poly(3,4-ethylenedioxythiophene) doped with poly(styrene sulfonate) (PEDOT:PSS) has been widely used in these devices, typically in the form of solid thin films. These films, while flexible, exhibit mechanical properties that differ significantly from soft biological materials, such as brain tissue. Hydrogels, by contrast, are intrinsically better suited to interfacing with soft, delicate biological materials. In this work, we investigate PEDOT:PSS-based hydrogels, for use as the top gate electrode in low-voltage hygroscopic insulator field effect transistors (HIFETs). We describe our method for fabricating patterned PEDOT:PSS hydrogel electrodes and report their electrical and rheological properties. We also show that HIFETs using PEDOT:PSS hydrogel gate electrodes exhibit good transistor characteristics and operate at low voltages ($-1\ V \leq V_{ds} \leq 0\ V$). Further, we demonstrate that hydrogel-gated HIFETs exhibit excellent sensitivity to aqueous potassium chloride (KCl) and sodium chloride (NaCl), as well as hydrogen peroxide (H_2O_2) over a range of concentrations. Lastly, we show that HIFET sensors can be translated to selective sensing of ions by demonstrating selective sensing of K^+ ions. Our results represent an important step forward in the development of HIFETs as soft and conformable sensors.

Introduction

Organic electronic devices for biosensors and bioelectronics have undergone rapid development in recent years. This includes the development of organic neural interfacing devices for recording brain activity,[1] the delivery of neurotransmitters for therapeutic purposes,[2] real-time stimulation of neural cells,[3] neural synaptic devices,[4] artificial retinas,[5] neuromorphic devices,[6] DNA sensors,[7] glucose sensors,[8] cortisol sensors,[9] and lactate sensors.[10,11] The applicability of organic devices to such a vast and diverse array of applications owes partly to their ability to be flexible and conformable, due to the inherent flexibility of organic semiconductors.[12,13] Additionally, organic semiconductors can be processed at low temperatures using solution processing methods and can be directly deposited into complex patterns using techniques such as inkjet printing.[14]

While a variety of organic electronic devices have been developed as biosensors, organic thin film transistors (OTFTs) have played a prominent role. OTFTs can amplify biological signals and can be functionalised to detect different analytes using selective membranes and intelligent device designs.[15–18]

Soniya D. Yambem

Soniya Yambem is a Senior Lecturer in Physics at the School of Chemistry and Physics, Queensland University of Technology (QUT). Soniya's research focusses on organic electronic devices, including organic photovoltaics, organic light emitting diodes and organic thin film transistors. She is interested in developing organic electronic devices for sensing, biosensing and bioelectronics. Soniya received her PhD from the University of Houston and then held a postdoctoral research fellowship at the University of Queensland. She then joined QUT as a Vice-Chancellor's Research Fellow, after which she transitioned into a lecturer position and got promoted to a Senior Lecturer.

[a] School of Chemistry and Physics, Faculty of Science, Queensland University of Technology (QUT), Brisbane, QLD 4000, Australia. E-mail: soniya.yambem@qut.edu.au
[b] Centre for Materials Science, Queensland University of Technology (QUT), Brisbane, QLD 4000, Australia
[c] Centre for Biomedical Technologies, Queensland University of Technology (QUT), Brisbane, QLD 4000, Australia

† Electronic supplementary information (ESI) available: Tables of figures of merit, additional figures. See DOI: https://doi.org/10.1039/d2tc01096h

A material widely used in OTFTs for biosensing and bioelectronics is poly(3,4-ethylenedioxythiophene) doped with poly(styrene sulfonate) (PEDOT:PSS).[19] PEDOT:PSS is a mixed electronic and ionic conductor and is therefore capable of transducing between ionic and electronic signals. PEDOT:PSS is also biocompatible, easily processable using simple methods such as spin coating and inkjet printing, and can be made stable in aqueous environments.[20] In OTFTs, PEDOT:PSS is primarily used as thin solid films, which have physical and mechanical properties that differ markedly from the properties of soft biological materials such as brain matter (Young's modulus 0.1–1 kPa).[21] In this respect, PEDOT:PSS in the form of a hydrogel is more compatible with very soft biological materials.[21,22]

There has been growing interest in conductive hydrogels for bioelectronics. Hydrogels are simply water-swelled three-dimensional networks of crosslinked polymers. They are soft, wet and conformable, providing a superior match in mechanical properties to soft tissues and organs, compared with rigid conventional electronics or even flexible, but solid, organic electronics.[23] Therefore, conductive hydrogels hold great promise in providing highly compatible electrical interfaces between electronics and biology.

Being a well-understood conducting polymer, PEDOT:PSS has been used extensively in conductive hydrogels. In some cases, PEDOT:PSS has been used as a conductive additive to an insulating hydrogel, called interpenetrating network hydrogels.[23–25] Alternatively, pure PEDOT:PSS hydrogels are formed by mixing water-based dispersions of PEDOT:PSS with crosslinking agents such as dimethyl sulfoxide (DMSO),[26] peptide–polyethylene glycol,[27] sulfuric acid,[28] or 4-dodecylbenzenesulfonic acid (DBSA).[22]

Some recent work has begun exploring PEDOT:PSS hydrogels as components in OTFTs. A pure PEDOT:PSS hydrogel fibre has been demonstrated as the channel material in an organic electrochemical transistor (OECT).[22] A PVA/PEDOT:PSS hydrogel has also been used as the electrodes (gate, source and drain) in a stretchable organic field effect transistor (OFET).[29] These reports show that PEDOT:PSS hydrogels can be successfully integrated into OTFTs. However, there is considerable need for further exploration in different device structures and applications to advance knowledge in this field.

In this work, we report pure PEDOT:PSS hydrogels as gate electrodes in hygroscopic insulator field effect transistors (HIFETs). HIFETs operate under low drain–source voltages ($-1\ \mathrm{V} \leq V_{ds} \leq 0\ \mathrm{V}$)[30] and have been explored as fully solid state sensors.[31–34] There have been many reports of HIFETs with thin solid films of PEDOT:PSS as the gate electrode,[35,36] including crosslinked films for stability in aqueous environments.[37] In this report, we take a step further and demonstrate the use of pure PEDOT:PSS hydrogels as the gate electrode for HIFETs. Hydrogel-gated HIFETs exhibit good low-voltage transistor characteristics, comparable to previously reported HIFETs with solid films of PEDOT:PSS as the gate electrodes. Further, we demonstrate that hydrogel-gated HIFETs are effective at sensing salt solutions, KCl and NaCl, across a wide range of concentrations (1 mM to 6 M) and H_2O_2 solutions (0.03 wt% to 30 wt%). We are also able to selectively detect K^+ by incorporating a K^+ selective membrane. Our demonstration of HIFET sensors with soft gate electrodes illustrates their suitability for soft electronic devices for biosensing and bioelectronic applications.

Experimental section

Fabrication

To prepare PEDOT:PSS hydrogel electrodes, a high conductivity formulation of PEDOT:PSS (Heraeus, Clevios PH 1000) was mixed with 4 v/v% DBSA (Sigma-Aldrich, 44198). DBSA at this concentration has been previously reported as an effective gelation agent for PEDOT:PSS.[22] The solution was then combined using a vortex mixer until the DBSA was thoroughly dispersed into the liquid (Fig. 1A). Thorough mixing is essential for the gelation of the hydrogel to proceed uniformly. Next, the solution was distributed into wells in a flexible polydimethylsiloxane (PDMS) mould. The mould was made by pouring a mixture of PDMS and curing agent into a 3D printed inverse mould and allowing to cure under vacuum. Each well had a length of 8 mm, a width of 2 mm and a depth of 1 mm, which are the intended dimensions of the final electrode. 15 μL of PEDOT:PSS solution was pipetted into each well (Fig. 1B). The entire mould was then sealed in a humid box for 1 hour at room temperature, to allow gelation to complete. Upon completion of gelation, each hydrogel electrode could be easily removed by simply bending the mould and using tweezers to lift the electrode away (Fig. 1C and D).

HIFETs were fabricated following well-established methods,[33,37] differing only with respect to the gate electrode. Glass slides with patterned 80 nm thick indium tin oxide (ITO) (Xin Yan Technology LTD.) for source and drain electrodes (with a third contact for the gate) were used. The channel between source and drain electrodes was 50 μm long and 3 mm wide. The slides were first scrubbed with acetone and then glassware detergent (Alconox), followed by ultrasonication in Alconox solution, deionised water, acetone and isopropanol for 10 minutes consecutively. The slides were dried after each step using compressed air. The clean substrates were spin coated with a 13 mg ml^{-1} solution of regioregular poly(3-hexylthiophene) (P3HT) (Rieke Metals, LLC, RMI-001EE) in a 1 : 1 mixture of chlorobenzene and chloroform at 3000 rpm for 30 seconds. This was followed by annealing at 60 °C for 10 minutes. Next, a dielectric layer of poly(4-vinylphenol) (PVP) (Sigma-Aldrich, 436224) was spin coated on the P3HT film from a solution in ethanol (80 mg ml^{-1}) at 2000 rpm for 1 minute, followed by annealing at 85 °C for 20 minutes. After each spin coating step, the films were manually patterned to expose the ITO contact pads for the gate, source and drain electrodes. Finally, a PEDOT:PSS hydrogel gate electrode was lifted into place directly from the PDMS mould onto the PVP layer of each HIFET, directly above the channel and in contact with the ITO gate contact pad on one end (see Fig. 3A). To minimise the dehydration of the electrodes in the drier ambient air, each individual HIFET was tested immediately

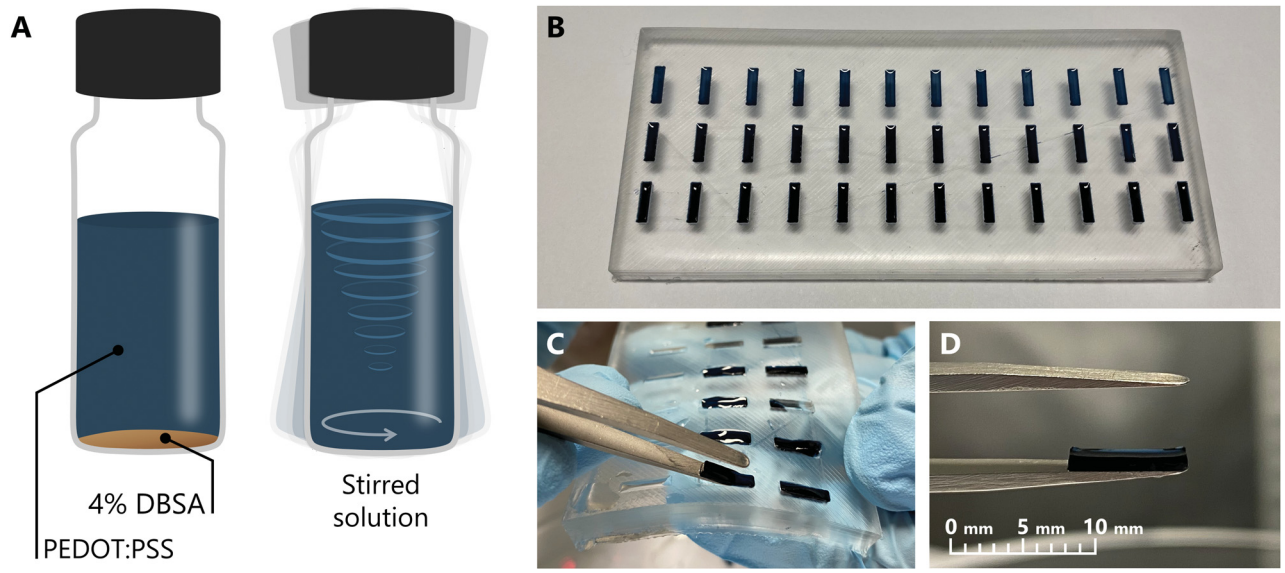

Fig. 1 The fabrication of PEDOT:PSS hydrogel electrodes. (A) Aqueous PEDOT:PSS suspension is combined with 4% (volume) DBSA, and then stirred using a vortex mixer. (B) The solution is deposited by pipette into wells in a PDMS mould. (C) Once gelation has occurred, the electrodes can be removed from the mould. (D) The electrode (8 mm × 2 mm × 1 mm) maintains the shape of the mould.

after its gate electrode was removed from the humid box and deposited.

Hydrogel-gated HIFETs selective to K^+ ions were fabricated by inserting PVC-based K^+ selective membranes between the gate and PVP layers of the HIFET. The membranes were fabricated by first combining the following in the indicated weight percentages: 2.5% K^+ ionophore III (Sigma-Aldrich, 60396), 60.5% diisodecyl adipate (Sigma-Aldrich, 460214), 0.5% potassium tetrakis(4-chlorophenyl)-borate (Sigma-Aldrich, 60591), and 36.5% poly(vinyl chloride) (Sigma-Aldrich). As it is difficult to accurately dispense small quantities of dry materials in precise ratios, solutions of 10 mg mL^{-1} K^+ ionophore, 10 mg mL^{-1} potassium tetrakis(4-chlorophenyl)-borate, and 75 mg mL^{-1} PVC in tetrahydrofuran (THF) were first prepared, which could be accurately dispensed using pipettes. The correct concentrations were finally reached by adding the remaining volume of THF needed to reach a concentration of 100 mg total material per 1 mL of THF. The solution was combined using a vortex mixer.

Membranes were fabricated by drop casting 30 μL of the solution onto cleaned glass slides, and dried at 50 °C for 10 minutes. The dry membranes were peeled off the glass and placed between the PVP and gate layers in HIFETs. The membranes were bonded to the PVP by first pipetting 2 μL of an adhesion promotor, 0.1% (v/v%) (3-glycidyloxypropyl)trimethoxysilane in deionised water, and gently pressing the membrane into place. Excess adhesive solution was removed using lint-free wipes. After allowing to dry, the hydrogel gate electrodes could be lifted into place onto the membranes to complete fabrication.

Characterisation

Current–Voltage (*I–V*) characteristics of hydrogel electrodes were obtained by placing the electrode between two ITO contacts with a separation of 3 mm (see inset in Fig. 2A) and sweeping the voltage between the contacts from −0.6 V to +0.6 V. Each electrode was measured twice. In general, the second measurements were more consistent than the first and these were used for the analysis. Conductance, and hence, conductivity was estimated from the slope of straight lines fitted to the *I–V* plots.

The rheological data for the PEDOT:PSS hydrogels were obtained using a rheometer (Anton Parr, M302 rheometer) with a 10 mm diameter parallel plate attachment. Sandpaper was glued to both plates to prevent slipping. 10 mm circular hydrogel samples were made using circular moulds in the same way as described above. Two samples were tested three times each to obtain representative averages. Two measurement types were performed: first, a frequency sweep from 0.01 to 10 rad s^{-1} where the complex viscosity was extracted; and second, a shear rate increasing test from 0.1% to 1% to compare the loss and storage moduli.

Standard output and transfer characteristics of HIFETs were recorded using a Keysight B1500A semiconductor analyser. For the transfer characteristics, gate voltage was swept at a rate of ≈70 mV s^{-1}. The sensitivity of hydrogel gated HIFETs to solutions of NaCl, KCl and H_2O_2 was tested by pipetting 5 μL of these analytes of varying concentrations onto the hydrogel gate electrode, directly above the channel. The drain–source current (I_{ds}) was recorded over time, while gate–source and drain–source voltage (V_g and V_{ds}) was fixed at −0.3 V and −1 V, respectively. These voltages were previously determined to be close to optimum for sensing ions in similar HIFETs.[34] Transfer characteristics were recorded before and after depositing the analyte to characterise the change in figures of merit. At least four separate devices were tested for each concentration. Unless specifically mentioned, all characterisations were done at room temperature.

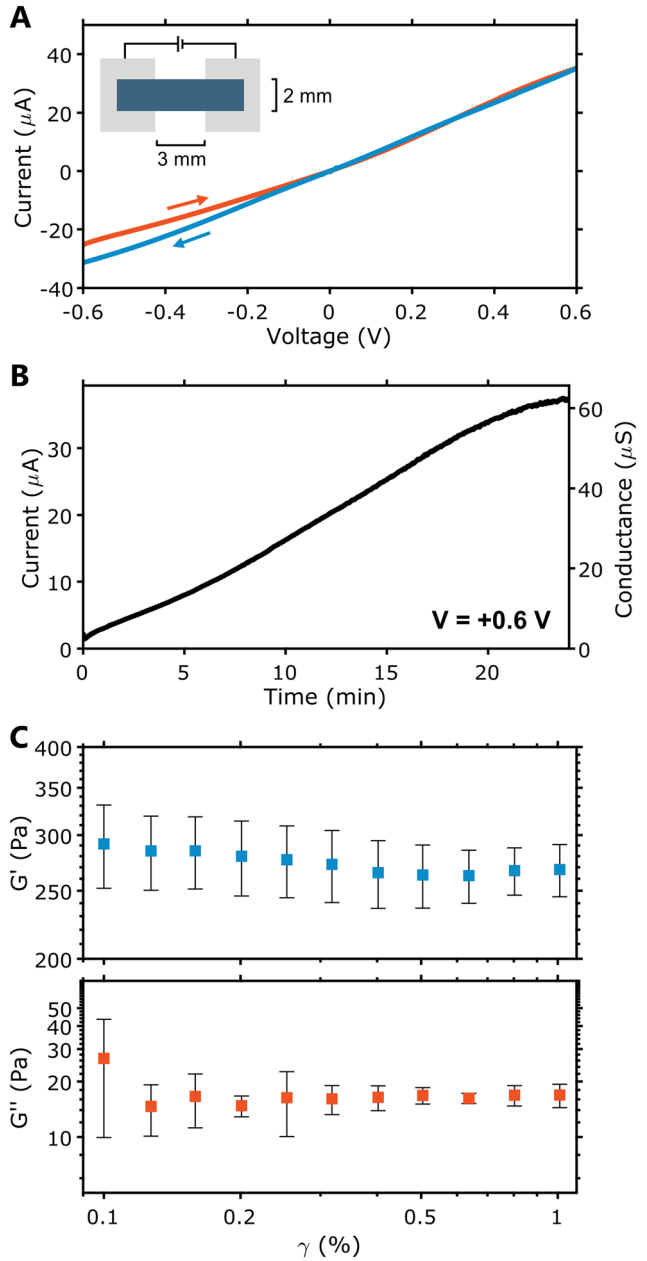

Fig. 2 (A) Representative current–voltage sweeps (forward and backward) for a PEDOT:PSS hydrogel electrode. The inset diagram shows the testing setup, where the hydrogel electrode (blue) is placed between two ITO contacts (grey) 3 mm apart, between which the voltage is applied. (B) The variation in the current and conductance of a hydrogel electrode over time (at a constant voltage of 0.6 V) under ambient conditions. (C) Average storage (G') and loss (G'') moduli for the PEDOT:PSS hydrogel, for sheer strain (γ) between 0.1% and 1%.

Results and discussion

Characteristics of PEDOT:PSS hydrogel electrodes

As shown in Fig. 1 and described in the Experimental Section above, we fabricated pure PEDOT:PSS hydrogels by adding 4% (v/v) DBSA to a commercial PEDOT:PSS dispersion, following a previously reported method.[22] Using a pure PEDOT:PSS hydrogel affords greater simplicity in fabrication. It also offers potentially better electrical characteristics, by avoiding the need for a secondary polymer matrix that might interrupt the conductive paths formed by the PEDOT:PSS.[23] Additionally, DBSA forms PEDOT:PSS hydrogels at room temperature, in contrast to various other approaches, further simplifying the process and making the procedure intrinsically more biocompatible.[22]

As indicated in the earlier study, the gelation of PEDOT:PSS in the presence of DBSA may be explained by the physical crosslinking of the PEDOT chains. The acidic DBSA could protonate the PSS, weakening the attraction between the PEDOT and PSS chains, thus allowing the PEDOT chains to interact and form physical interchain bonds *via* hydrophobic attraction and π–π stacking.[22]

We found the PEDOT:PSS hydrogel could be readily formed to the desired dimensions by using PDMS moulds (Fig. 1B), and, once formed, is sufficiently robust to maintain its shape while being moved and manipulated with tweezers (Fig. 1D). For the gate electrodes, we chose to use an 8×2 mm^2 area, the same as previously reported thin film gate electrodes for HIFETs,[37] and a thickness of 1 mm. Thinner hydrogel electrodes were tested, but are more fragile and difficult to consistently remove from the mould without incurring damage.

The conductance of these PEDOT:PSS hydrogel electrodes was determined from current–voltage (I–V) characteristics. Fig. 2A displays a representative example. Individual I–V characteristics for all samples are given in Fig. S1A (ESI†). Comparing the forward and backward voltage sweeps (Fig. 2A), some hysteresis is evident, reflecting dynamic processes within the hydrogel, likely involving the movement of ions. Across a length of 3 mm (cross section = 2 mm^2), the hydrogel electrodes exhibited an average conductance of 55 ± 16 μS, and thus a conductivity of 83 ± 24 mS m^{-1}. This conductance is well above that of thin film PEDOT:PSS electrodes used in earlier HIFETs ($\approx$ 7 μS)[36] and so is more than sufficient for use as gate electrodes.

When left in the ambient environment, the electrical characteristics of the hydrogel change over time. Fig. 2B plots the current and conductance of a hydrogel electrode over time, under ambient conditions. The current at a fixed voltage (0.6 V) was recorded continuously for 24 minutes, starting with a 'fresh' sample immediately after it was removed from the humid box in which it had been stored for curing. The conductance of the electrode clearly increases significantly over time (26× larger after 24 minutes), during which the hydrogel visibly dried and contracted. Mass loss due to drying proceeds linearly (see Fig. S1B, ESI†), at a rate of -0.2 mg min^{-1} (humidity $\sim$45%, temperature $\sim$22 °C). After 24 minutes, mass is reduced by $\sim$50%. The reduction in the proportion of water in the hydrogel as it dries increases the PEDOT:PSS density and hence its conductance increases. This phenomenon may have an impact on the characteristics of hydrogel-gated HIFETs operating in ambient conditions. To minimise this impact during standard testing procedures, we stored each hydrogel electrode inside a humid box until they were ready to be transferred to a HIFET, and immediately tested.

The rheological properties of the PEDOT:PSS hydrogel were tested within its linear region (where shear strain, γ, is $<1\%$). The storage modulus (G') and loss modulus (G'') for the PEDOT:PSS hydrogel can be seen in Fig. 2C. G' characterises the energy stored and is associated with elastic properties, whereas G'' characterises the energy dissipated and is associated with viscous properties.[38,39] In Fig. 2C, it is evident that G' is significantly larger than G''. This is represented by the loss factor ($\tan\delta$), which is the ratio of G'':G' (Table S2, ESI†). At 0.5% shear strain, we record a low $\tan\delta$ of 0.1 ± 0.1. This points to strong elastic behaviour in the hydrogel, as values closer to 0 indicate more elastic behaviour. A $\tan\delta$ between 0 and 1 is considered to indicate "solid-like" behaviour.[40] Fig. S2A (ESI†) shows that the complex viscosity (η^*) decreases with an increase in angular frequency (ω) which is characteristic of physically crosslinked hydrogels.[22] Additionally, we found that hydrogel samples preserved by immersion in water for 24 hours retain gel properties, while being subject to increases in G', G'', $\tan\delta$ and η^* compared to fresh samples (see Fig. S2A and B, ESI†). This may suggest additional crosslinking occurs over longer periods. Overall, these analyses show that our pure PEDOT:PSS hydrogels are soft elastic gels. Similar gels, reported previously, exhibited comparable properties and were also found to have a very low Young's modulus ($\approx$1 kPa), on the lowest end of the range seen in human tissue.[22]

PEDOT:PSS hydrogel-gated HIFETs

The feasibility of using PEDOT:PSS hydrogels as gate electrodes for HIFETs was tested using the simple, solution processable structure shown in Fig. 3A. This HIFET structure has been shown to operate within low voltage ranges, which is important for biosensors and bioelectronics.[30] The source and drain electrodes are ITO and there is a third ITO contact pad for the gate. This gate contact pad acts as a bridge between the PEDOT:PSS hydrogel and the probe used to deliver the gate voltage. A well-studied organic semiconductor, P3HT is used as the channel material and hygroscopic insulator PVP is used as the dielectric layer. Being hygroscopic, the PVP layer retains moisture and functions as a solid-state electrolyte. The device functionality is thus analogous to an electrolyte-gated organic field effect transistor (EGOFET). The low voltage properties arise from the high capacitance of electrical double layers formed at the PVP interfaces. The chemical structure of all the materials used in the HIFET including DBSA and PEDOT:PSS are shown in Fig. 3B.

Representative output and transfer characteristics for a HIFET with a PEDOT:PSS hydrogel gate are shown in Fig. 3C and D, respectively. These show good transistor characteristics at low V_g and V_{ds}, comparable to previously reported HIFETs using solid PEDOT:PSS gate electrodes. The output curves exhibit well-defined linear and saturation regimes, and the I_{ds}

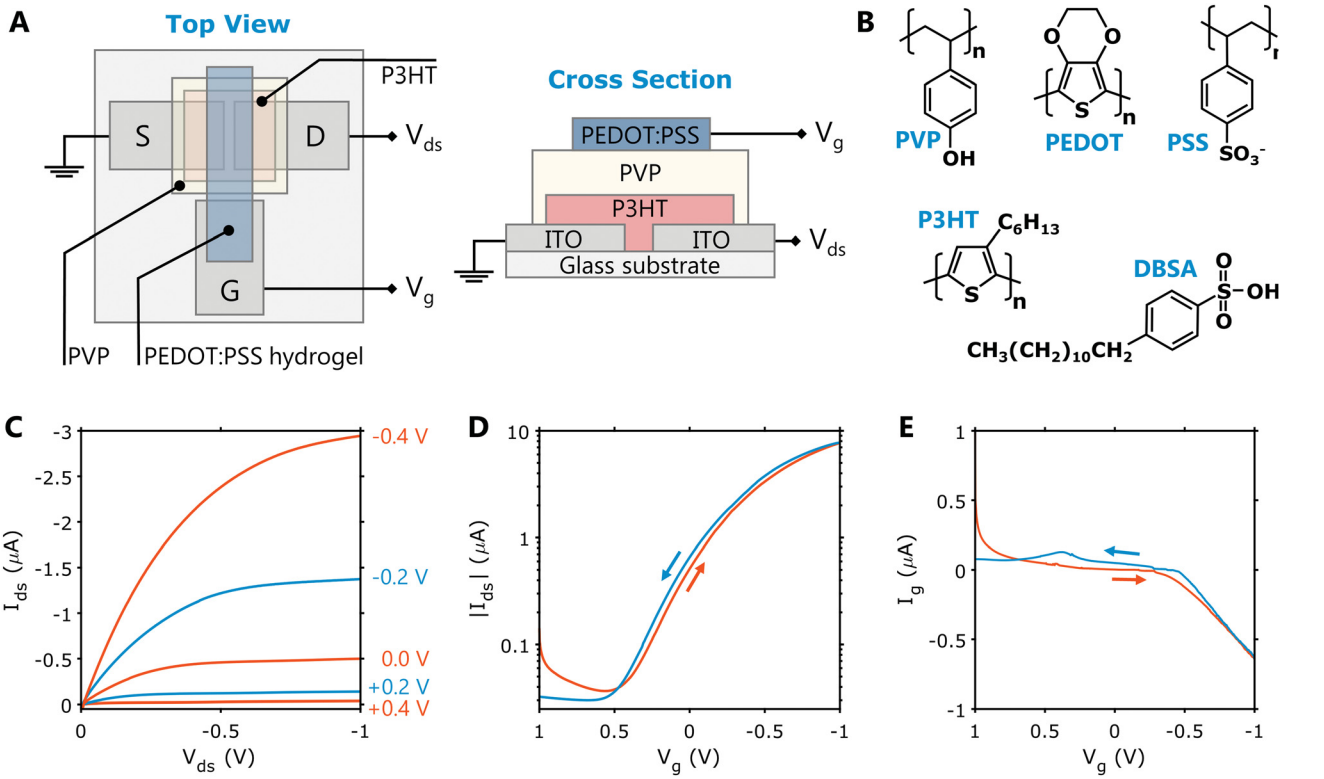

Fig. 3 (A) HIFET device structure, showing top and cross-sectional views (not to scale). (B) Chemical structures of main components of the PEDOT:PSS hydrogel-gated HIFETs: PVP, P3HT, PEDOT, PSS and DBSA. (C) Representative output characteristics for hydrogel-gated HIFETs, each curve recorded for a different V_g between +0.4 V and −0.4 V. (D) Representative forward and back transfer sweep, for V_{ds} = −1 V. (E) Gate current (I_g) recorded during the transfer sweep shown in (D).

is well modulated by the gate voltage. The transfer curves also show minimal hysteresis between forward and backward sweeps at a moderate sweep rate ($\approx$ 70 mV s^{-1}). Repeated testing over a period slightly increases the ON current and non-ideal characteristics in the $+V_g$ regime. The changing characteristics of the gate electrode over time (Fig. 2B) is the likely cause of this observation. Testing at faster sweep rates (up to $\approx$550 mV s^{-1}) yield virtually no change in the hysteresis (Fig. S4, ESI†).

Figures of merit (see Table S1, ESI† for description) are extracted from the transfer sweeps (negative to positive sweep) for each device tested (see Table S5, ESI†). In a batch of 19 devices, the average ratio of the ON and OFF currents was 160 $\pm$ 50, with an average ON current of -7 ± 2 μA, and an OFF current of -0.05 $\pm$ 0.02 μA. The average transconductance (g_m), which characterises how well a change in V_g can modulate I_{ds}, was 2.9 $\pm$ 0.8 μS mm^{-1}. The gate leakage current at $V_g = V_{ds} = -1$ V varied considerably between devices, giving an average of -1.0 ± 1.6 μA.

Overall, the figures of merit for HIFETs with hydrogel gates are comparable to HIFETs we have reported previously that used solid PEDOT:PSS gate electrodes crosslinked with divinyl sulphone. In those devices, the ON/OFF ratio was 150 $\pm$ 20 (ON = -8.7 ± 0.8 μA, OFF = -0.06 ± 0.01 μA), and the transconductance was 3.6 $\pm$ 0.4 μS mm^{-1}. Gate current at $V_g = V_{ds} = -1$ V was -0.1 ± 0.1 μA. Thus, the primary difference caused by the use of hydrogel gates was increased gate leakage current and poorer consistency between individual devices within a batch. The increased gate leakage possibility arises from the acidity of the wet hydrogel gate, infiltrating the PVP dielectric and increasing its conductivity. The poor consistency is likely related to the gate leakage, as well as any variations in the electrical characteristics of the gate. With regard to the effect on overall transistor characteristics, however, these weaknesses are relatively minor and the PEDOT:PSS hydrogel electrodes therefore show to be highly effective for gating HIFETs.

Sensing characteristics

HIFETs using solid crosslinked PEDOT:PSS films as gate electrodes have been shown to be sensitive to a range of biologically relevant analytes, including H_2O_2,[33] NaCl, KCl, HCl and NaOH.[34] To evaluate the capabilities of PEDOT:PSS hydrogel-gated HIFETs for biosensing applications, here we have tested their sensitivity to NaCl, KCl and H_2O_2 across a wide range of concentrations.

Fig. 4 shows the sensing characteristics of hydrogel-gated HIFETs for KCl (A–D), NaCl (E–H), and H_2O_2 (I–L). For each test, constant voltages were applied ($V_g = -0.3$ V and $V_{ds} = -1$ V), and the I_{ds} was measured over time. After allowing the I_{ds} to stabilise, 5 μL of the analyte was deposited onto the hydrogel gate electrode (at t = 0 seconds). The modulation of the I_{ds} is defined as the percentage change to the I_{ds} with respect to the initial current immediately prior to introducing the analyte: $100 \times [I_{ds}(t) - I_{ds}(0)]/I_{ds}(0)$.

Representative I_{ds} modulations for KCl, NaCl and H_2O_2 are given in Fig. 4A, E and I, respectively. Modulations for individual samples are provided in the ESI† (Fig. S5–S7, ESI†). The average maximum modulations are plotted in Fig. 4B, F, and J. The transfer characteristics for each HIFET were also recorded before and after testing the analyte, allowing us to observe how the figures of merit change with concentration. The modulations in ON current and transconductance are plotted in Fig. 4C, D, G, H, K and L. Plots showing absolute values for these figures of merit are given in Fig. S8 (ESI†).

Varying concentrations of both salts were tested. For KCl, concentrations as low as 0.01 M gave clear and positive modulations in I_{ds}. For NaCl, an additional lower concentration, 0.001 M, was tested and could also be detected with a modulation in I_{ds}. High-concentration samples (4 M and 6 M), close to the maximum solubility of the respective salts, were included to show the maximum possible responses. At equivalent molar concentrations, HIFETs respond very similarly to both NaCl and KCl solutions, indicating that there is no intrinsic ion selectivity. Differences in ion size, hydration and mobility do not have a significant effect on the I_{ds} modulation. On a log–log scale, plots of I_{ds} modulation are linear through all concentrations tested, allowing for straightforward calibration (see Fig. S9, ESI†).

Since all analytes are aqueous, it was also important to characterise the effect of deionised water (0 M). This indicates the baseline response due to additional hydration of the HIFET by the analyte solution and represents the theoretical minimum response. These HIFETs exhibited relatively minor changes in response to water. A small response to water is ideal for sensors intended to detect aqueous analytes, as the 'background' signal due to the water in the sample will not overwhelm the signal due to the ions. Thus, all concentrations that were tested can be readily distinguished from water, including the 0.001 M analyte (for NaCl). Using the background response and fitted calibration equations, the limit of detection (95% confidence interval) is estimated to be 0.0016 M for KCl and 9.7×10^{-5} M for NaCl. The poorer detection limit for KCl results from the larger standard deviation in the 0 M data for that particular batch of devices. Given the variability inherent in the HIFET fabrication process, the variation in the sensitivity of HIFETs can be large. However, the data for the NaCl tests shows low standard deviations are possible, and this can likely be achieved consistently with refinement of the fabrication process.

The cations Na^+ and K^+ are normally present in human blood serum in concentrations of 0.135–0.145 M and 0.0035–0.0055 M, respectively. Thus, our hydrogel-gated HIFETs are sensitive to biologically relevant levels of Na^+.

The sensitivity of these hydrogel-gated HIFETs is similar to HIFETs with solid PEDOT:PSS films reported previously.[34] The absolute magnitudes of the I_{ds} modulations are very similar. For example, 1 M NaCl causes I_{ds} modulations of 100 $\pm$ 7% using the hydrogel gate electrodes, while the devices with solid gates gave modulations of 102 $\pm$ 4%. The close correspondence of these results shows that the hydrogel gate electrode does not fundamentally change the ion sensitivity of the underlying HIFET. However, when using the solid electrodes, the I_{ds} modulations were not clearly distinguished from water until

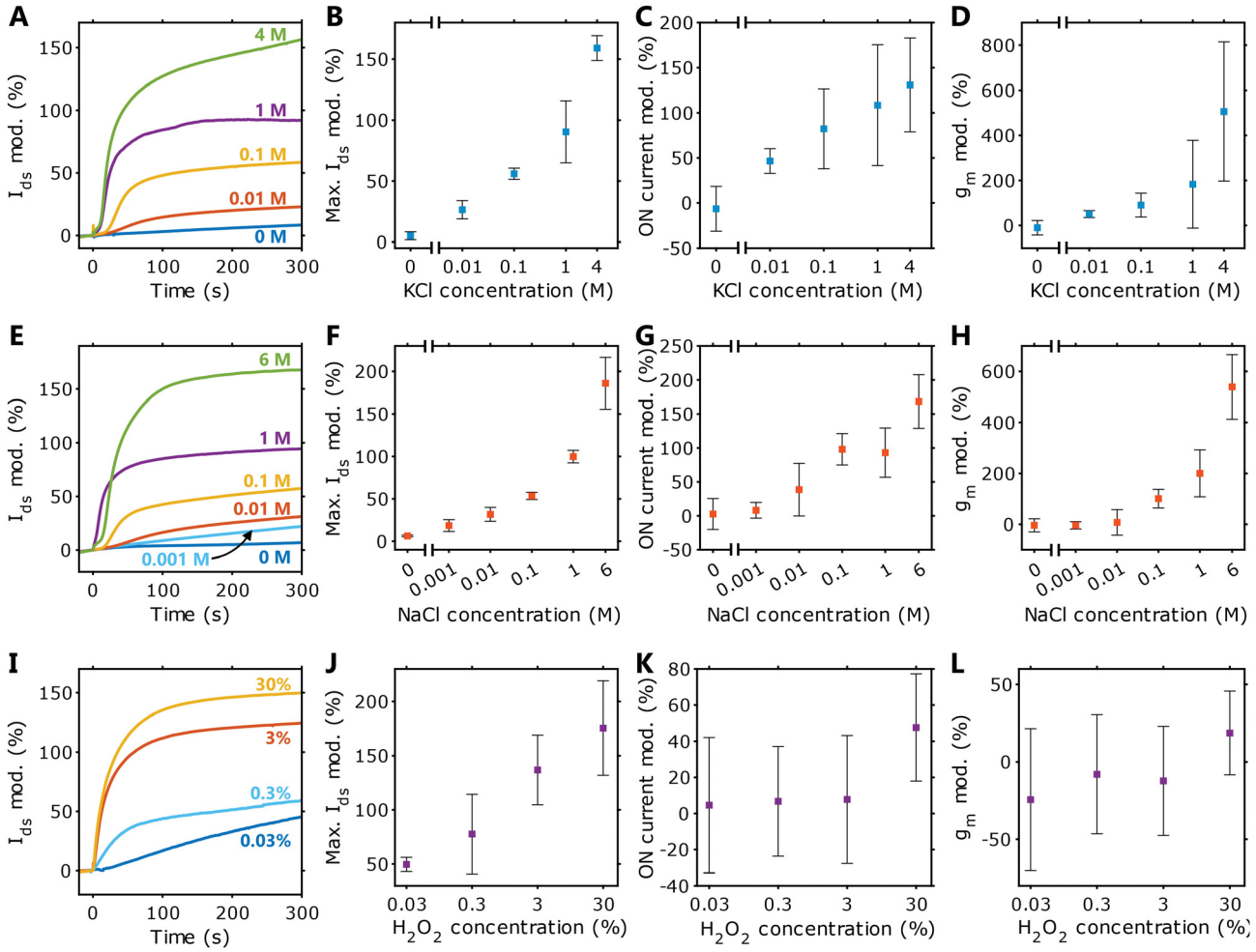

Fig. 4 (A) Representative transient I_{ds} modulations for PEDOT:PSS hydrogel-gated HIFETs, upon deposition of 5 μL of KCl solutions at t = 0 s. (B) Average maximum I_{ds} modulations (±S.D.) for various KCl concentrations. (C and D) Average modulation in ON currents and transconductances (g_m) of HIFETs after depositing KCl solutions of various concentrations. (E) Representative transient I_{ds} modulations for HIFETs, upon deposition of 5 μL of NaCl solutions at t = 0 s. (F) Average maximum I_{ds} modulations (±S.D.) for various NaCl concentrations. (G and H) Average modulation in ON currents and transconductances (g_m) of HIFETs after depositing NaCl solutions of various concentrations. (I) Representative transient I_{ds} modulations for HIFETs, upon deposition of 5 μL of H_2O_2 solutions at t = 0 s. (J) Average maximum I_{ds} modulations (±S.D.) for various H_2O_2 concentrations (wt%). (K and L) Average modulation in ON currents and transconductances (g_m) of HIFETs after depositing H_2O_2 solutions of various concentrations.

concentrations were above 0.01 M. In those devices, greater sensitivity could only be achieved by calculating the transconductance and other figures of merit, which were able to distinguish concentrations as low as 0.001 M.[34] Being able to sense these concentrations directly using the change in I_{ds} is a notable advantage of the hydrogel-gated HIFETs. The difference may be attributed to the initial hydration levels of the devices with the different gate electrodes. The wet hydrogel electrodes allow the underlying PVP layer to become thoroughly hydrated prior to testing, so the overall hydration of the device does not significantly change when an analyte is added. The HIFETs with solid-state gates were comparatively drier, so the absorption of water from the analyte had a significant effect on device performance, therefore masking the smaller effect of the ions.

Regarding the figures of merit for hydrogel-gated HIFETs, we see that both the ON current and transconductance increase significantly with analyte concentration. This shows that the added ions are improving overall transistor performance. Additional figures of merit are provided in Tables S7 and S9, in the ESI.†

The effect of NaCl and KCl on HIFETs using PEDOT:PSS hydrogel gates is consistent with the ion sensing mechanism for HIFETs we proposed earlier.[34] The ions deposited onto the hydrogel gate electrode rapidly diffuse through the gate and into the PVP layer. The additional ions increase the effective ionic strength of the hydrated PVP layer, increasing the capacitance of the device. With increased capacitance, the transconductance of the transistor is increased and greater charge is accumulated for a given V_g, resulting in the observed increase in I_{ds}.

Hydrogel-gated HIFETs are also clearly sensitive to H_2O_2. H_2O_2 is vital for enzyme-based biosensors, as it is produced as a by-product of the enzymatic oxidation of molecules such as glucose. Thus, sensors with H_2O_2 sensitivity are applicable for a

broad range of biosensing applications. The I_{ds} modulations (Fig. 4I–J) show that hydrogel-gated HIFETs respond to a range of H_2O_2 concentrations, comparable to previous results observed with solid gate electrodes.[33]

After sensing H_2O_2, neither the ON current nor the transconductance change significantly for concentrations below 30 wt%. The large error bars (representing one standard deviation) reflect the significant variation experienced observed in the effects on individual devices (Fig. 4K–L). Other figures of merit are provided in Table S11 (ESI†). This is a very different effect compared with the salt analytes, reflecting a difference in underlying sensing mechanisms. We have previously studied H_2O_2 sensing in HIFETs and proposed that the analyte causes the oxidation of the P3HT channel, increasing its baseline conductivity.[33]

Ion selectivity

HIFETs can be considered to be general sensing platforms, with intrinsic sensitivity to a broad variety of ions. However, in most real-world applications, it is necessary to distinguish between different ions present in a solution. A common way to achieve ion selectivity in OTFTs is to employ ion-selective membranes. As a proof-of-concept that our HIFETs can be easily translated into ion selective sensors, we here demonstrate a K^+ selective hydrogel-gated HIFET sensor. K^+ selectivity was achieved by inserting a K^+ selective membrane between the gate and PVP layer. In this structure, the PVP layer is equivalent to the "inner filling solution" used in many OECT and EGOFET sensors that employ ion-selective membranes.[41,42]

Output and transfer characteristics for hydrogel-gated HIFETs using K^+ selective membranes show good transistor characteristics with clear current modulations at low voltages (see Fig. S10, ESI†). Average ON/OFF ratio and transconductance are however reduced to 70 ± 10 and 1.9 ± 0.4 μS mm^{-1}, respectively with the inclusion of K+ membrane (see Table S12 (ESI†) for additional figures of merit). Nevertheless, it is clear that HIFETs can be gated through the membrane.

Fig. 5A shows representative I_{ds} modulations upon deposition of 1 M KCl, 1 M NaCl and deionised water (data for each trial is provided in Fig. S11, ESI†). While water alone produces a small, negative modulation ($-8 \pm 6\%$ on average), NaCl typically results in a small positive response ($7 \pm 7\%$). The small response to 1 M NaCl differs notably from the large modulation in Fig. 4E, showing that the membrane largely prevents the infiltration of the NaCl into PVP layer. In response to 1 M KCl, there is a significant, negative I_{ds} modulation ($-24 \pm 7\%$). This is clearly distinct from the response to NaCl, showing that selective detection of K^+ ions is achieved. The negative modulation in I_{ds} is indicative of a fundamentally different detection mechanism than is seen in HIFETs without the membrane (compare Fig. 4A and 5A).

Without the membrane (Fig. 5B), both K^+ and Cl^- from the analyte infiltrate the PVP, adding to the existing anions and cations within the HIFET. The increased ionic strength enhances the effective gate voltage by increasing the device capacitance, giving a positive I_{ds} modulation (Fig. 4A). With the membrane (Fig. 5C), potassium ionophores embedded in the membrane selectively bind with K^+ ions from the analyte (Cl^- cannot pass the membrane). As positive charge from the analyte accumulates, the membrane potential increases (positively). The membrane potential (E_m) is often modelled using

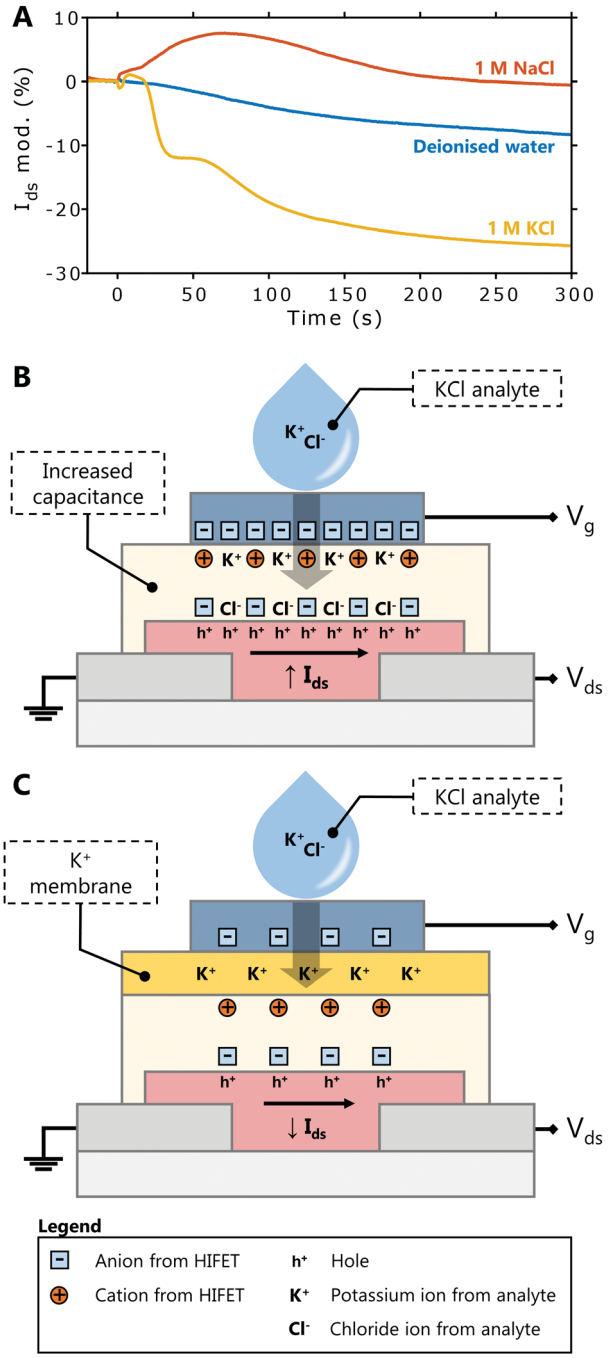

Fig. 5 (A) Representative transient I_{ds} modulations for PEDOT:PSS hydrogel-gated HIFETs with K^+ selective membranes, upon deposition of 5 μL of deionised water, 1 M NaCl and 1 M KCl. (B) The ion sensing mechanism without the K^+ selective membrane. Ions from the deposited analyte diffuse through the gate electrode and into the PVP dielectric, where device capacitance is increased, increasing I_{ds}. (C) The ion sensing mechanism with the K^+ selective membrane. K^+ ions accumulate in the membrane, changing the effective gate voltage and decreasing I_{ds}.

the Nernst equation (eqn (1)), where E_0 is a constant, R is the universal gas constant, T is the temperature, z_i is the valency of the ion, F is Faraday's constant, and a is the ion activity in the analyte or inner filling solution.[41]

$$E_m = E_0 + \frac{RT}{z_i F}\ln\left(\frac{a_{analyte}}{a_{inner}}\right) \quad (1)$$

The ''effective gate voltage'' that drives the formation of electrical double layers in the PVP is the sum of the applied gate voltage and the electrolyte potential.[41] The applied gate voltage, −0.3 V, means the device is initially in an 'on' state, with anions accumulated at the P3HT interface and mobile holes in the P3HT channel. As the membrane potential becomes more positive due to K^+ in the membrane, this counteracts the negative gate voltage, and the net effective gate voltage is more positive. As a result, the number of anions accumulated at the P3HT interface is reduced, and the hole density in the channel is reduced as well, decreasing the magnitude of I_{ds} (Fig. 5A).

Our results demonstrate that ion selective membranes can be straightforwardly integrated into hydrogel-gated HIFET sensors to achieve ion selectivity. This represents a first step towards HIFET-based multifunctional biochips to simultaneously test for a variety of ions on a single substrate. Further work is necessary to first optimise the sensitivity of these devices. Since ion-selective HIFETs rely on changes to the effective gate voltage, a high transconductance is likely needed to maximise amplification of the signal. Transconductance increases with gate thickness,[36] likely due to increasing capacitance, but rapidly plateaus. In using a very thick gate electrode in this experiment, further increasing gate capacitance would have little effect. Further steps for optimisation may include increasing channel width with interdigitated electrodes to increase I_{ds}, and optimising membrane thickness. Different ion-selective membranes can be incorporated to different devices on a single substrate to make a multifunctional biochip. Alternative scalable methods of fabrication, such as inkjet printing, will allow easy patterning and fabrication of more complex and integrated devices. It is also important to investigate means to robustly adhere the hydrogel to the underlying device, which is a limitation of the work presented here.

Conclusions

We have demonstrated that PEDOT:PSS hydrogel can be used as effective gate electrodes for HIFET ion sensors. Geometrically defined hydrogel electrodes can be formed at room temperature by mixing DBSA with a PEDOT:PSS dispersion, and allowing to crosslink in PDMS moulds. These electrodes exhibit a good conductivity of $\approx$80 mS m^{-1}, and rheological characteristics typical of a soft, elastic hydrogel. These electrodes can then be used directly as the gate electrode for simple, solution-processed HIFETs. Hydrogel-gated HIFETs exhibit good transistor characteristics, with minimal hysteresis. The ON/OFF ratio and transconductance of these devices is comparable to previously reported HIFETs using solid crosslinked PEDOT:PSS gate electrodes. We also find that hydrogel-gated HIFETs are excellent ion sensors, responding with modulations in I_{ds} to a range of KCl and NaCl concentrations, down to 0.001 M, as well as H_2O_2. We finally showed that HIFETs are platform devices that can be customised for ion selectivity by incorporating an ion-selective membrane and demonstrated a K^+ sensitive HIFET. Overall, we demonstrated that pure PEDOT:PSS hydrogels have great potential to serve as gate electrodes for HIFET-based sensors for interfacing with biology.

Author contributions

J. N. A. and S. D. Y. drafted the manuscript. S. B. conducted the primary investigation, including HIFET fabrication, characterisation, and sensing tests. Q. T. B conducted initial trials. J. N. A. collected the hydrogel I–V data, and conducted the K^+ selective membrane experiments. C. M. C. performed the rheological experiments and analysis. S. B., Q. T. B. and J. N. A. developed the methodology. J. N. A. provided data analysis. S. D. Y. conceptualised and supervised the project. All authors reviewed the manuscript.

Conflicts of interest

There are no conflicts of interest to declare.

Acknowledgements

The authors acknowledge the Central Analytical Research Facility (CARF) at the Queensland University of Technology (QUT) for training and access to various analytical instruments. S.D.Y. would like to acknowledge funding from the Advanced Queensland Women's Research Assistance Program (WRAP) (WRAP078-2019RD1).

References

1 D. Khodagholy, J. N. Gelinas, Z. F. Zhao, M. Yeh, M. Long, J. D. Greenlee, W. Doyle, O. Devinsky and G. Buzsaki, *Sci. Adv.*, 2016, **2**, 8.
2 A. Jonsson, Z. Y. Song, D. Nilsson, B. A. Meyerson, D. T. Simon, B. Linderoth and M. Berggren, *Sci. Adv.*, 2015, **1**, 6.
3 V. Benfenati, S. Toffanin, S. Bonetti, G. Turatti, A. Pistone, M. Chiappalone, A. Sagnella, A. Stefani, G. Generali, G. Ruani, D. Saguatti, R. Zamboni and M. Muccini, *Nat. Mater.*, 2013, **12**, 672–680.
4 Q. Z. Liu, Y. H. Liu, J. Li, C. Lau, F. Q. Wu, A. Y. Zhang, Z. Li, M. R. Chen, H. Y. Fu, J. Draper, X. Cao and C. W. Zhou, *ACS Appl. Mater. Interfaces*, 2019, **11**, 16749–16757.
5 M. Ciocca, P. Giannakou, P. Mariani, L. Cinà, A. Di Carlo, M. O. Tas, H. Asari, S. Marcozzi, A. Camaioni, M. Shkunov and T. M. Brown, *Sci. Rep.*, 2020, **10**, 21457.
6 T. N. Mangoma, S. Yamamoto, G. G. Malliaras and R. Daly, *Adv. Mater. Technol.*, 2020, **7**, 2000798.
7 M. Demelas, S. Lai, G. Casula, E. Scavetta, M. Barbaro and A. Bonfiglio, *Sens. Actuators, B*, 2012, **171**, 198–203.

8 T. Mano, K. Nagamine, Y. Ichimura, R. Shiwaku, H. Furusawa, H. Matsui, D. Kumaki and S. Tokito, *Chem-ElectroChem*, 2018, **5**, 3881–3886.
9 O. Parlak, S. T. Keene, A. Marais, V. F. Curto and A. Salleo, *Sci. Adv.*, 2018, **4**, eaar2904.
10 L. J. Currano, F. C. Sage, M. Hagedon, L. Hamilton, J. Patrone and K. Gerasopoulos, *Sci. Rep.*, 2018, **8**, 11.
11 A. M. Pappa, D. Ohayon, A. Giovannitti, I. P. Maria, A. Savva, I. Uguz, J. Rivnay, I. McCulloch, R. M. Owens and S. Inal, *Sci. Adv.*, 2018, **4**, eaat0911.
12 M. S. White, M. Kaltenbrunner, E. D. Głowacki, K. Gutnichenko, G. Kettlgruber, I. Graz, S. Aazou, C. Ulbricht, D. A. M. Egbe, M. C. Miron, Z. Major, M. C. Scharber, T. Sekitani, T. Someya, S. Bauer and N. S. Sariciftci, *Nat. Photonics*, 2013, **7**, 811.
13 M. Kaltenbrunner, T. Sekitani, J. Reeder, T. Yokota, K. Kuribara, T. Tokuhara, M. Drack, R. Schwödiauer, I. Graz, S. Bauer-Gogonea, S. Bauer and T. Someya, *Nature*, 2013, **499**, 458–463.
14 S. Chung, K. Cho and T. Lee, *Adv. Sci.*, 2019, **6**, 1801445.
15 N. X. Wang, A. N. Yang, Y. Fu, Y. Z. Li and F. Yan, *Acc. Chem. Res.*, 2019, **52**, 277–287.
16 J. Rivnay, S. Inal, A. Salleo, R. M. Owens, M. Berggren and G. G. Malliaras, *Nat. Rev. Mater.*, 2018, **3**, 14.
17 D. T. Simon, E. O. Gabrielsson, K. Tybrandt and M. Berggren, *Chem. Rev.*, 2016, **116**, 13009–13041.
18 E. Macchia, K. Manoli, B. Holzer, C. Di Franco, M. Ghittorelli, F. Torricelli, D. Alberga, G. F. Mangiatordi, G. Palazzo, G. Scamarcio and L. Torsi, *Nat. Commun.*, 2018, **9**, 3223.
19 M. Berggren, X. Crispin, S. Fabiano, M. P. Jonsson, D. T. Simon, E. Stavrinidou, K. Tybrandt and I. Zozoulenko, *Adv. Mater.*, 2019, **31**, 15.
20 S. Stříteský, A. Marková, J. Víteček, E. Šafaříková, M. Hrabal, L. Kubáč, L. Kubala, M. Weiter and M. Vala, *J. Biomed. Mater. Res., Part A*, 2018, **106**, 1121–1128.
21 J. Liu, H. Zheng, P. S. P. Poh, H.-G. Machens and A. F. Schilling, *Int. J. Mol. Sci.*, 2015, **16**, 15997–16016.
22 S. Zhang, Y. Chen, H. Liu, Z. Wang, H. Ling, C. Wang, J. Ni, B. Çelebi-Saltik, X. Wang, X. Meng, H.-J. Kim, A. Baidya, S. Ahadian, N. Ashammakhi, M. R. Dokmeci, J. Travas-Sejdic and A. Khademhosseini, *Adv. Mater.*, 2020, **32**, 1904752.
23 H. Yuk, B. Lu and X. Zhao, *Chem. Soc. Rev.*, 2019, **48**, 1642–1667.
24 V. R. Feig, H. Tran, M. Lee and Z. Bao, *Nat. Commun.*, 2018, **9**, 2740.
25 Y.-F. Zhang, M.-M. Guo, Y. Zhang, C. Y. Tang, C. Jiang, Y. Dong, W.-C. Law and F.-P. Du, *Polym. Test.*, 2020, **81**, 106213.
26 B. Lu, H. Yuk, S. Lin, N. Jian, K. Qu, J. Xu and X. Zhao, *Nat. Commun.*, 2019, **10**, 1043.
27 Y. Xu, X. Yang, A. K. Thomas, P. A. Patsis, T. Kurth, M. Kräter, K. Eckert, M. Bornhäuser and Y. Zhang, *ACS Appl. Mater. Interfaces*, 2018, **10**, 14418–14425.
28 B. Yao, H. Wang, Q. Zhou, M. Wu, M. Zhang, C. Li and G. Shi, *Adv. Mater.*, 2017, **29**, 1700974.
29 J.-C. Ho, Y.-C. Lin, C.-K. Chen, L.-C. Hsu and W.-C. Chen, *Org. Electron.*, 2022, **100**, 106358.
30 H. G. O. Sandberg, T. G. Bäcklund, R. Österbacka and H. Stubb, *Adv. Mater.*, 2004, **16**, 1112–1115.
31 S. D. Yambem, J. Timm, M. Weiss, A. K. Pandey and R. Marschall, *Adv. Electron. Mater.*, 2017, **3**, 1700316.
32 D. Elkington, W. J. Belcher, P. C. Dastoor and X. J. Zhou, *Appl. Phys. Lett.*, 2014, **105**, 4.
33 J. N. Arthur and S. D. Yambem, *Adv. Mater. Technol.*, 2021, 2101149.
34 J. N. Arthur and S. D. Yambem, *ACS Appl. Electron. Mater.*, 2022, **4**, 842–849.
35 T. G. Bäcklund, H. G. O. Sandberg, R. Österbacka and H. Stubb, *Appl. Phys. Lett.*, 2004, **85**, 3887–3889.
36 J. N. Arthur, M. U. Chaudhry, M. A. Woodruff, A. K. Pandey and S. D. Yambem, *Adv. Electron. Mater.*, 2020, **6**, 9.
37 J. N. Arthur, C. M. Cole, A. K. Pandey and S. D. Yambem, *J. Mater. Chem. C*, 2021, **9**, 8169–8178.
38 C. D. Han and M. S. Jhon, *J. Appl. Polym. Sci.*, 1986, **32**, 3809–3840.
39 A. B. Kousaalya, B. I. Biddappa, S. Rai and S. Pilla, in *Biocomposites*, ed. M. Misra, J. K. Pandey and A. K. Mohanty, Woodhead Publishing, 2015, pp. 161–200, DOI: **10.1016/B978-1-78242-373-7.00016-0**.
40 T. T. H. Pham, S. V. Vadanan and S. Lim, *Cellulose*, 2020, **27**, 8075–8086.
41 K. Schmoltner, J. Kofler, A. Klug and E. J. W. List-Kratochvil, *Adv. Mater.*, 2013, **25**, 6895–6899.
42 S. Han, S. Yamamoto, A. G. Polyravas and G. G. Malliaras, *Adv. Mater.*, 2020, **32**, 2004790.